

Conceptual detector development and Monte Carlo simulation of a novel 3D breast computed tomography system

Jens Ziegler¹, Bernhard H. Müller¹, Bernd Neumann¹, Christoph Hoeschen^{1,2}
¹Otto-von-Guericke University Magdeburg, Institute of Medical Engineering
²Helmholtz Zentrum München German Research Center for Environmental Health,
Research Unit for Medical Radiation Physics and Diagnostics

ABSTRACT

A new 3D breast computed tomography (CT) system is under development enabling imaging of microcalcifications in a fully uncompressed breast including posterior chest wall tissue. The system setup uses a steered electron beam impinging on small tungsten targets surrounding the breast to emit X-rays. A realization of the corresponding detector concept is presented in this work and it is modeled through Monte Carlo simulations in order to quantify first characteristics of transmission and secondary photons. The modeled system comprises a vertical alignment of linear detectors held by a case that also hosts the breast. Detectors are separated by gaps to allow the passage of X-rays towards the breast volume. The detectors located directly on the opposite side of the gaps detect incident X-rays. Mechanically moving parts in an imaging system increase the duration of image acquisition and thus can cause motion artifacts. So, a major advantage of the presented system design is the combination of the fixed detectors and the fast steering electron beam which enable a greatly reduced scan time. Thereby potential motion artifacts are reduced so that the visualization of small structures such as microcalcifications is improved. The result of the simulation of a single projection shows high attenuation by parts of the detector electronics causing low count levels at the opposing detectors which would require a flat field correction, but it also shows a secondary to transmission ratio of all counted X-rays of less than 1 percent. Additionally, a single slice with details of various sizes was reconstructed using filtered backprojection. The smallest detail which was still visible in the reconstructed image has a size of 0.2mm.

Keywords: breast imaging, 3D breast imaging, microcalcifications, Geant4 simulation, detector design

1 INTRODUCTION AND DESCRIPTION OF PURPOSE

Microcalcifications in the breast can be an early indicator of breast cancer, in particular if they show certain patterns. These calcifications are below a size of one millimeter and have a high X-ray attenuation coefficient compared to the surrounding breast tissue. Therefore X-ray imaging systems with high spatial resolution become important diagnostic tools to detect and localize microcalcifications. X-ray mammography systems provide 2D images of compressed breast showing the attenuation of superimposed tissue structures. Thus, in 2D projection images the superimposition of radiographically dense tissues potentially cover abnormal structures like calcifications, but also conversely creates artifacts which can lead to misinterpretation in the diagnosis [1].

The introduction of breast tomosynthesis enabled the visualization of slices by taking several X-ray projections from limited different angles of the compressed breast. Therefore, a 3D reconstruction of the acquired data set reduces the effect of superimposed structures which enhances the distinction between tissues [2]. Breast tomosynthesis, however, does not allow a full visualization of the breast volume including posterior tissues towards the chest wall and the compression of the breast may still cause misinterpretation in detected lesions. The resolution in the z-direction is typically much coarser than in the plane.

In the past years several 3D breast imaging developments were introduced allowing the visualization of the breast volume without the need of a breast compression [3][4]. In principle, at a prone position of the patient with one breast hanging in a container, the X-ray source and the detector rotate around the breast acquiring the imaging data. The obtained three-dimensional information of the breast tissue with a high resolution flat-panel detector improves the image

resolution and thus the localization of microcalcifications.

However some systems lack the visualization of important structures posterior to the chest wall. Additionally, the mechanical movement of the source and the detector can increase the acquisition time potentially leading to artifacts due to patient motion.

In order to prevent motion artifacts a new 3D breast imaging CT is under development. To avoid mechanically moving parts, the source consists of concentrically fixed small anodes surrounding a containment holding the breast volume. A fast steering electron beam hits each of the fixed anodes leading to the emission of X-rays towards the breast volume. The presented corresponding detector design in this work comprises vertically fixed detector stripes around the containment sidewalls. This setup also allows imaging of a non-compressed breast at patients prone position given the possibility to visualize the full breast volume including posterior chest wall structures.

The aim of this work is to evaluate a conceptual detector design in order to assess first characteristics of primary and secondary X-rays, i.e. transmission and scattering plus X-ray fluorescence, respectively. The system setup and the conceptual detector design was modeled in a Monte Carlo simulation which provides quantitative information about the transmission and secondary X-ray photon process in the irradiated parts of the detector and electronics. Thereby the effect of the proposed materials and detector arrangements on the spatial and spectral distribution of transmission and secondary X-rays is analyzed.

2 MATERIAL AND METHODS

2.1 Imaging setup and conceptual detector design

In figure 1a a schematic diagram in a longitudinal section of the system setup is shown, given an electron beam source tilted to impinge on small needle-like anode targets within a high-vacuum container. A cross sectional top view of the system is provided in figure 1b showing the concentrically aligned anode targets in the outer ring. The system heats a tungsten filament with a heating current up to 150 mA for electron emissions. A formed electron beam hits each of 255 targets with a radial frequency of 1 kHz. The emitted X-rays have a maximum energy of 40 keV and pass through a 2 mm thick aluminum case in the direction of the breast, as shown in figure 1a. This setup had been manufactured by the Fraunhofer Institute for Organic Electronics, Electron Beam and Plasma Technology.

The conceptual detector design constitutes vertically aligned linear detector stripes on the inner sidewalls of the aluminum case. The detector stripes are supposed to be separated with gaps next to each other. This allows the passage of X-rays through the gaps and through a container that holds the breast. The detector stripes that are located directly on the opposite side of the gaps then detect the attenuated X-rays, as shown in figure 1b. It is also shown that between the gaps at the backside of the detectors the incident X-rays are blocked by the highly absorbing detectors interconnection structures intended for signal transmissions which are depicted in figure 1c. Thus, the interconnection structures shield the linear sensor elements of the detector from unwanted X-ray exposure at the backside. A polymer material is used as substrate for the interconnection structures and as holder for the detector stripes. Both are interconnected via a gold wire and the sensor elements are covered with cesium-iodide as scintillator material.

2.2 Monte Carlo simulations of the imaging setup with the conceptual detector design

A Monte Carlo simulation of the imaging setup consisting of the previously described geometry has been developed using the Geant4 Monte Carlo toolkit [5]. There the electron beam and anode targets were assumed to be point-like X-ray sources at the positions of single anode targets. The source creates a cone beam with an X-ray spectrum of a 2mm Al-filtered 40 kVp X-ray tube. The spectrum has been calculated using the program SpekCalc (version 1.1)[6]. A number of 3.67×10^{10} X-ray photons was used in the Monte Carlo simulation. A curved geometry was implemented using an ideal area detector with an energy bin size of 0.1 keV as depicted in figure 1a and b which records transmitted and scattered X-rays as well as X-ray fluorescence. Thus, the spatially and spectrally resolved distribution of the transmitted and secondary X-rays were acquired. The summation of the spectrum at each point of the area detector forms a single projection image of the irradiated geometries.

Besides the simulation of the complete system including the detector design, the system was also simulated without the detector design including only the aluminum case and breast container. The resulting spectra from the simulation without the detector design were used as standard reference data in order to quantify influences of the detector design on the

characteristics of transmitted and secondary X-rays. Hereby, a transmission and secondary ratio for each energy bin was calculated by the division of the photon counts within the detector design simulation to the counts within the standard reference simulation.

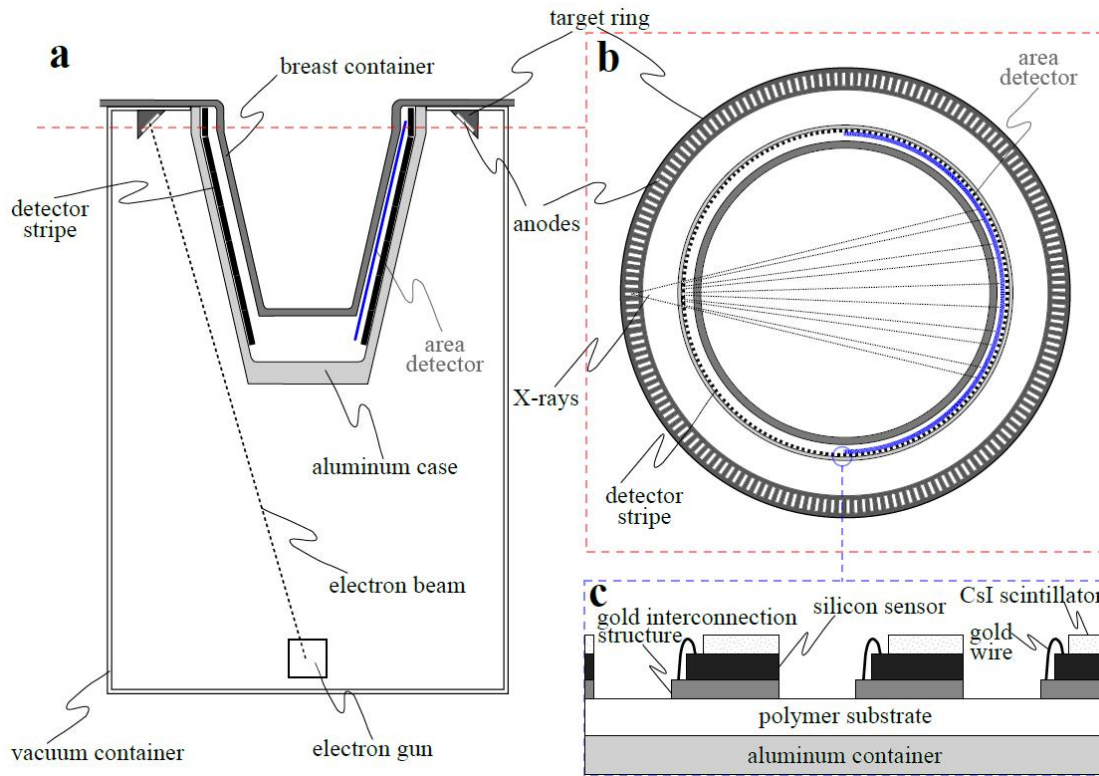


Figure 1: a) Longitudinal section of the system setup. b) Cross sectional top view of the concentrically system alignment and an example X-ray beam. c) Simulated hardware components of the detector design.

2.3 Reconstruction of simulated Radon data for a single slice

Radon data of a single slice using the proposed detector design were acquired by Monte Carlo simulation of the x-ray transport using Geant4 simulation toolkit in order to estimate the resolution capacity in its reconstructed image. Cylindrical details with diameters of 5mm, 2.5 mm and 1mm were simulated as polymethyl methacrylate (PMMA) with a density that is equivalent to breast tissue. Also details with diameters of 0.5mm, 0.2mm and 0.05mm of hydroxyapatite that is mainly calcium phosphate for equivalence to microcalcifications were simulated. The details were placed as shown in figure 2.

For single slice data fan-beams with 26keV energy were used. This energy was chosen because of its high probability of occurrence in an X-ray spectrum with a maximum energy of 40keV out of a tungsten filament. Each center of the 255 anodes was defined as the origin of a point-source on a 10.4cm radius around the coordinate center and emitted a fan-beam with an opening angle of 60 degree in direction to the details, i.e. the center beam of the fan was aligned to the center of the coordinate system. Consequently, 255 rotations steps were available to create the Radon data. Therefore the angular rotation step size was set to 1.42 degree. The number of X-ray photons per rotation step was set to 3.67×10^8 .

The volume of the scintillator on each detector stripe was implemented as an ideal detector. For each rotation step all ideal detectors were read out which contained the raw data for image reconstruction. Further, in MATLAB the fan-beam sections in the raw data were cut out to form the raw fan-beam sinogram. Due to beam divergence a normalization was applied using a reference raw fan-beam sinogram out of a second simulation without detail placements. MATLAB's *iradon()* function was used for the reconstruction with filtered backprojection. Since this function uses equidistant projection data the raw fan-beam sinogram had to be rebinned into parallel-beam data. Therefore, a rebinning method according to the detector geometries was implemented where a bilinear interpolation was required. After transformation

the image of the single slice was reconstructed using the default settings of the *iradon()* function. In the reconstructed image the smallest visible detail gives the first impression of the resolution capacity for the proposed detector design.

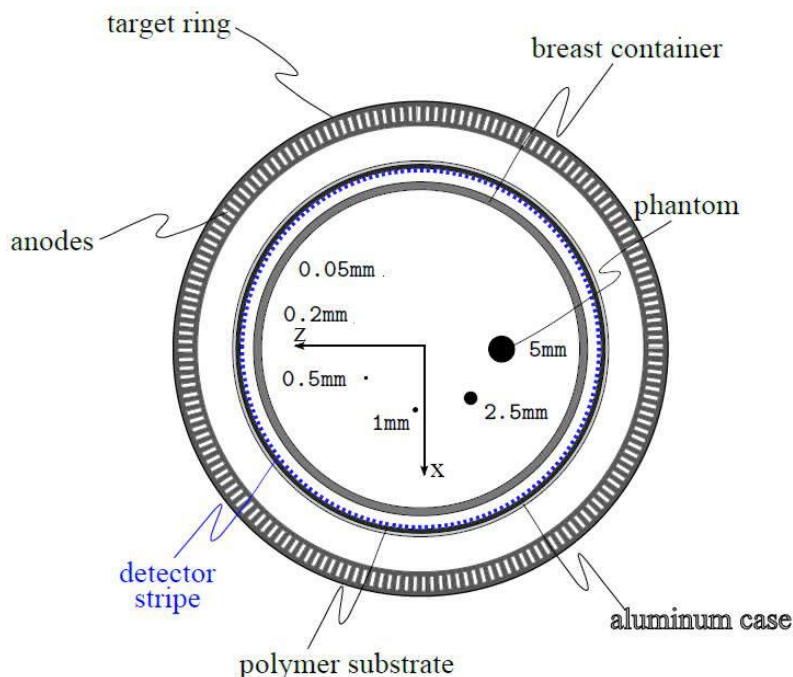


Figure 2: Simulated geometries including details for slice reconstruction to estimate the resolution capacity. Each anode center represents the origin of a simulated mono-energetic X-ray fan-beam. The scintillator on the detector stripes was implemented as ideal detectors to record the raw data for the reconstruction.

3 RESULTS AND DISCUSSION

In figure 3a the transmission and secondary X-ray spectra, i.e. scattering plus X-ray fluorescence for the latter, of the simulations with and without the detector design is shown. The counts for transmission with the detector geometries result in a general decrease. The integration of all counts in both transmission spectra shows a reduction of 25.2%, i.e. this amount of transmission photons were either absorbed, scattered or result into fluorescence. Figure 3b more clearly shows the dependence of the number of transmitted X-rays on the energy where the transmission ratio is plotted for each energy bin. The transmission ratio is always below 1 except for very low energies where the uncertainties due to the low statistics give values above 1. At energy 11.7 keV the number of transmission count is lower than 10 photons and therefore statistically negligible. In contrary, the amount of secondary photons in the low energy range is increased as clearly shown in the secondary ratios in figure 3c. Here, in the range from 9.3 keV to ~15 keV the high secondary ratios are caused by the gold *L*-fluorescence at the *L*-absorption edges. Thus, the detector materials increase the amount of scattered X-rays and fluorescence in the volume of the breast case. This increases the energy dose deposited in the breast by a small factor which could be reduced by placing the detector element on the outside of the aluminum breast case, so that the aluminum is used as a filter. But in general the ratio of all scattering counts to all transmission counts is 0.2% and thus the forward scattering is comparably low.

The ratio for the transmitted primary photons within the spectrum, representing the non-scattered X-ray fraction, is 54.4 % of all emitted photons. The ratio of the forward scattered photons is 3.3 %. Thus, 42.3 % of all emitted photons were not detected. Since the ideal area detector did not cover each angle in the system's volume, a part of scattered photons, e.g. back-scattered ones were not detected. However, a certain amount of photons had been absorbed by the detector materials.

An extraction of the recorded image at the area detector is shown in figure 4. The image presents the ratio of the number

of transmitted photons resulting from the simulation including the detector design in place to the number of transmitted photons from the simulation without the detector design. As expected, areas with a ratio down to zero represent the positions of the interconnection lines where the linear sensor element are shielded. The zero ratios cover 15.9 % of the whole projection image, i.e. represents the amount of totally absorbed photons. Areas with a transmission ratio of 100% represent the gaps between the detector stripes. Conversely, they describe the acquired data of detector stripes placed on the opposite side to the gaps. Within those areas, it can be seen that the interconnecting wires lead to lower signals, as indicated by lower transmission ratios. Consequently, a flat-field correction via a post-processing method would be required for those regions.

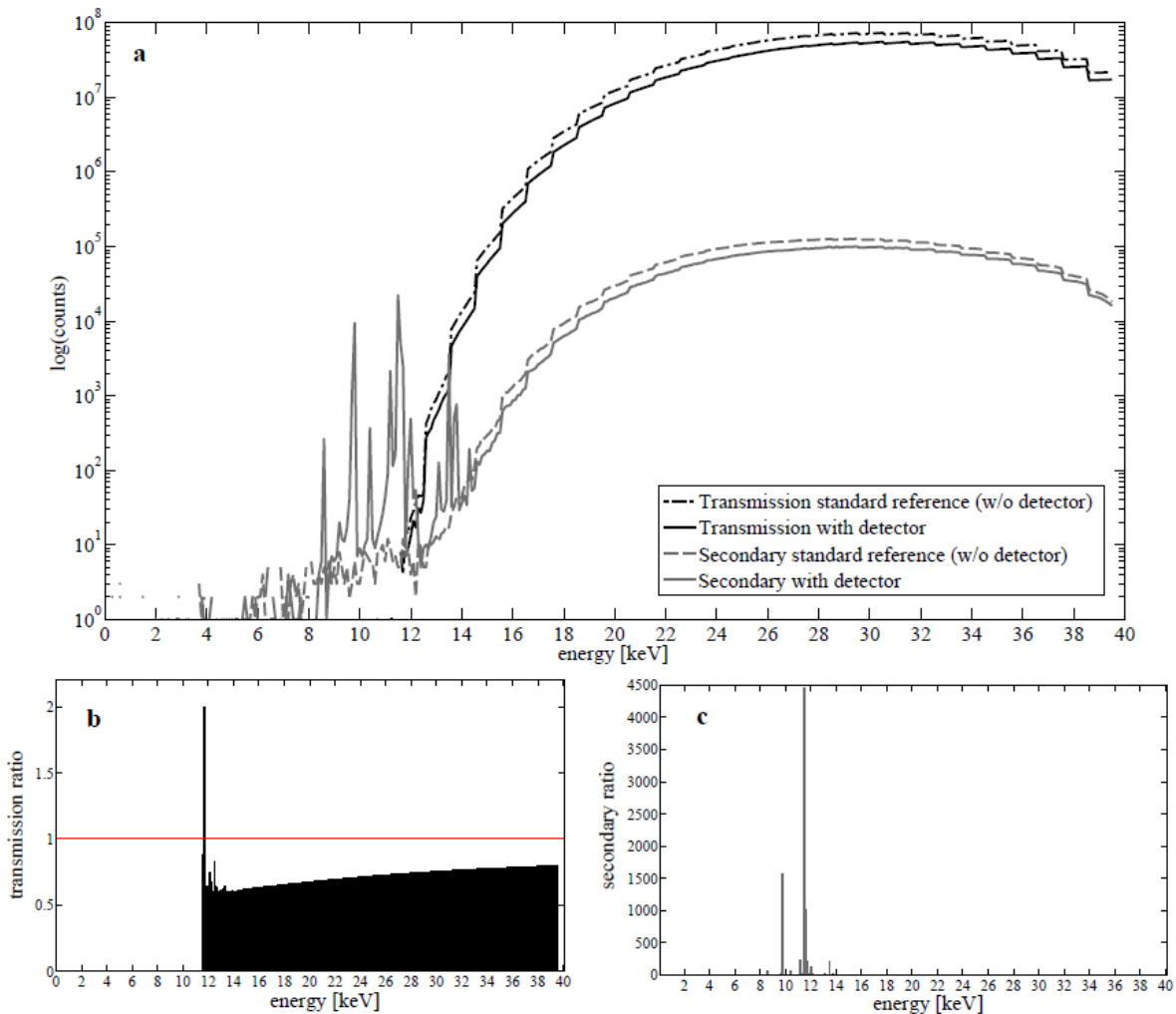


Figure 3: a) Transmission and secondary X-ray spectra in photon counts per energy for simulation with and without the detector geometry in logarithmic scale. b) Energy dependent transmission ratios for all energies of detected primary photons. c) Energy dependent secondary ratios for all energies of detected scattering and fluorescence photons. Ratios of the spectra are given in number of counts with the detector geometries to the number of counts without the detector geometries, i.e. the standard reference spectra.

Figure 5 illustrates the results of the raw data processing steps. The raw data contains the number of counts in the projections at all detector elements for each rotation step. The counts resulting from all incident X-rays are shown, i.e. for the elements at the opposite side which passed through the volume of the breast container including the details. The latter are cut to yield the raw fan-beam sinogram in which the sinograms of the details can be observed. Additionally, it shows some black pixels which indicate non-irradiated detector elements caused by the structures on the ingress blocking the fan-beam as described previously and shown in Figure 4. Also the beam divergence can be seen, which,

however, is corrected by normalization using the raw fan-beam reference data resulting in a homogenous intensity distribution along the number of detector elements and reveals clearly gaps in some sinograms. The gaps at some rotation steps can occur when projections of an object are smaller than the gap size between the detector elements and are directed to the gaps, and thus they are not detected. In the rebinning process the black pixels were skipped to avoid false bi-linear interpolations and so were substituted by the interpolation.

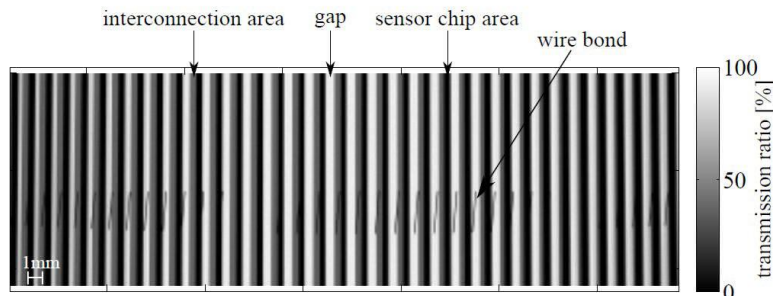


Figure 4: Spatial transmission ratio depending on the detector geometry. Areas with low ratio indicate the detector stripes positions and high ratios represent the gaps between the detector stripes. The wire structure that is proposed to connect the sensor elements with the interconnection data lines reduces the transmission ratio.

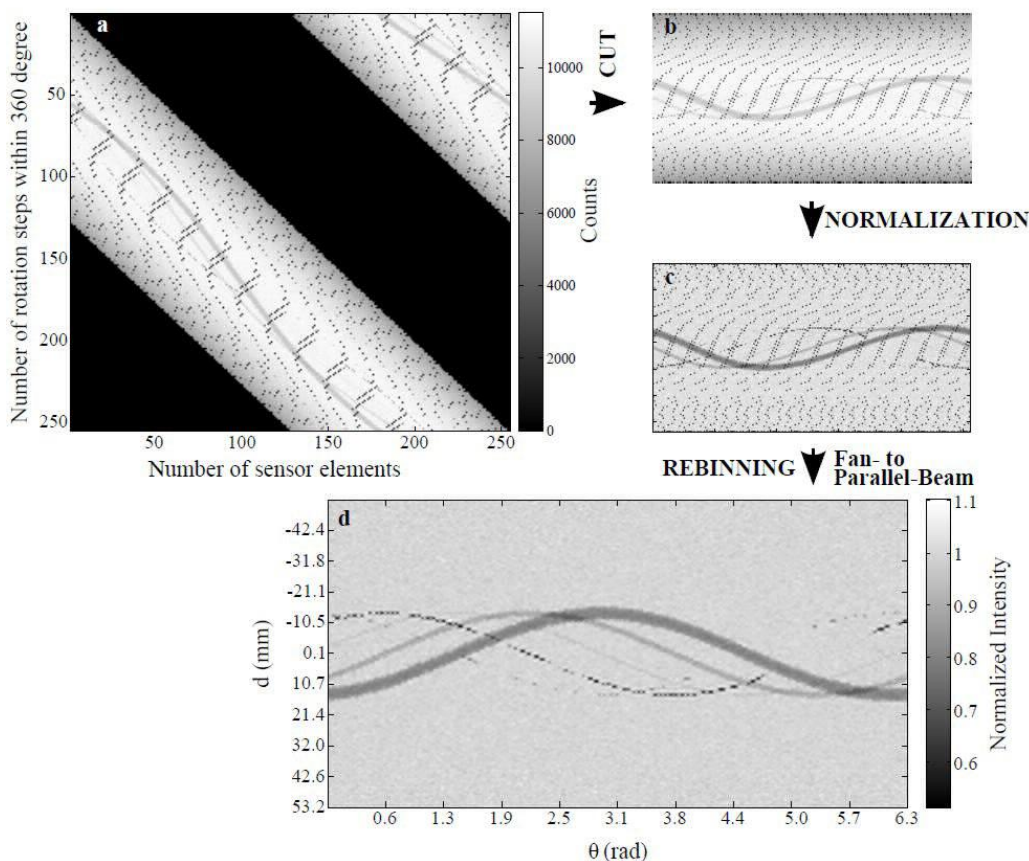


Figure 5: Raw data processing to obtain equidistant sinogram of Radon data for reconstruction. a) Raw data of all detector elements for each rotation step that is cut to b) raw fan-beam sinogram. c) A normalization with raw fan-beam sinogram of reference data results into normalized fan-beam sinogram. The rebinning converts the fan-beam sinogram into d) equidistant parallel-beam sinogram including equidistant Radon data. Here theta is the angle between coordinate axis and parallel beam and d is the orthogonal distance from the parallel beam to the coordinate center.

The reconstructed image of a single slice is shown in figure 6. The 5mm, 2.5mm PMMA and 0.5mm microcalcification details are clearly visible. But also the 1mm PMMA and 0.2mm microcalcification details appear slightly. The reconstructed 0.5mm detail results in streak artifacts over the whole image around itself which is likely caused by its high attenuating density compared to the surrounding. Also the detector elements are not directly positioned next to each other, thus the intermediate gaps do not result in an ideal sampling. These facts as well as the gaps in this detail's sinogram lead to problems in the filtered backprojection. The streak artifacts are a result of the gaps and the non-uniformity of the sampling of the sinogram in combination with an unoptimized rebinning procedure and the partial volume effect [7]. Also to prevent artifacts caused by non-uniformity of the sampling an other reconstruction algorithm based on orthogonal polynomial expansion on the disk (OPED)[8] can be applied as given with a comparable detector arrangement in a CT with dual optimal reading (CT d'Or)[9]. The diameters of the 5mm and 2.5mm details were obtained in pixels and a mean conversion factor of 82.81×10^{-3} mm/pixel was calculated to relate the pixel to the original size. This resulted in an estimated field of view of 58.8mm x 58.8mm for a fan-beam with an opening angle of 60 degree.

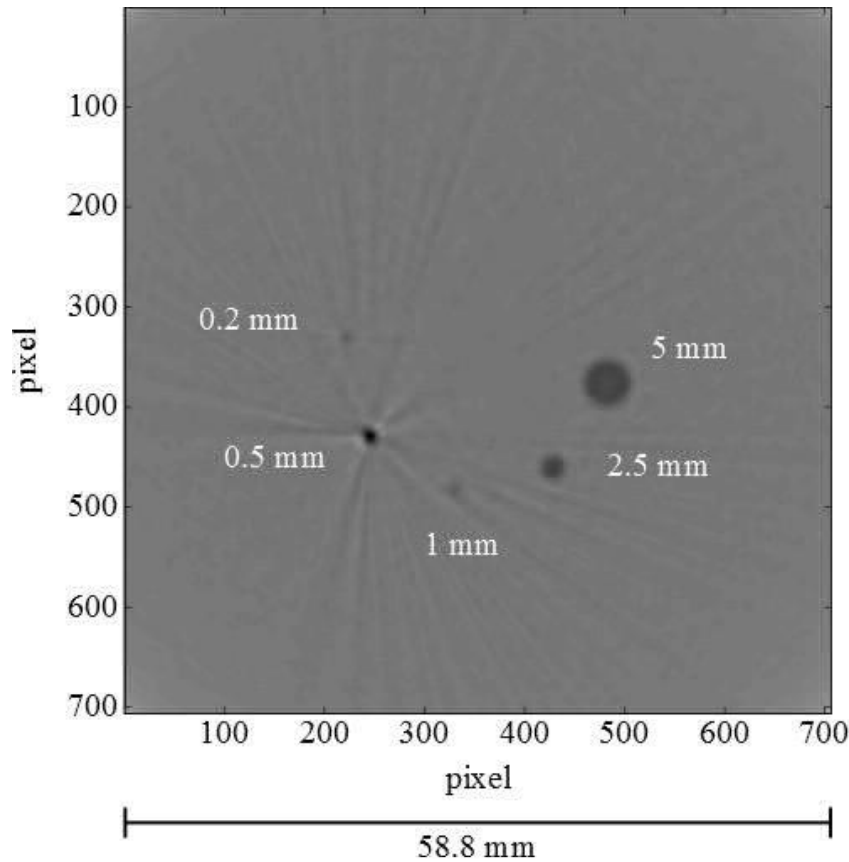


Figure 6: Reconstructed single slice containing cylindrical details with sizes of 5mm, 2.5mm, 1mm PMMA equivalent to breast density and 0.5mm and 0.2mm calcium phosphate as material similar micro-calcifications. 0.5mm detail showing streak artifacts known as partial volume artifact [5].

4 NEW WORK AND CONCLUSION

In this work a new 3D breast computed tomography system that uses a steered electron beam impinging on small anodes surrounding the breast volume for X-ray emission has been presented. A detector design for this system consisting of concentrically aligned detector stripes around the breast volume has been

developed and first characteristics of the influence of the detector elements on the spectral and spatial distribution of X-rays have been quantified. Using a Monte Carlo simulation it is shown that the presented detector design does not lead to high levels of forward scattering which resulted from the irradiation of the detector elements. Furthermore, the reduction of the transmissions are mainly caused by absorption of the detector's electrical interconnection structures. Hereby, it is shown that flat-field correction would be necessary. The remaining part of the incident photons are sufficient to create enough projections for a reconstruction of a single slice using a filtered backprojection method. The visibility of the 0.2mm sized detail gives an estimate of the resolution performance of this first prototype of a breast CT system. However, the proposed detector design results in a nonuniform sampling of the sinograms with gaps depending on the distance between the edges of the detector elements which leads to artifacts in the reconstruction for objects smaller than the size of these gaps. This problem, however, could be reduced by a different, more tightly packed, detector arrangement in combination with an optimized rebinning procedure. Despite the non-uniformly sampling, this detector design for the MammoScan 6/40 system highlights a promising approach for the detection of microcalcifications in the breast.

7 REFERENCES

- [1] Rafferty, E. A., Park, J. M., Philpotts, L. E., Poplack, S. P., Sumkin, J. H., Halpern, E. F. and Niklason, L. T., "Assessing Radiologist Performance Using Combined Digital Mammography and Breast Tomosynthesis Compared with Digital Mammography Alone: Results of a Multicenter, Multireader Trial", *Radiology*, Radiological Society of North America (RSNA), 266, 104-113 (2013).
- [2] Kopans, D., Gavenonis, S., Halpern, E. and Moore, R., "Calcifications in the Breast and Digital Breast Tomosynthesis", *The Breast Journal*, Wiley-Blackwell, 17, 638-644 (2011).
- [3] Kalender, W. A., "Concepts for high-resolution CT of the breast", *Digital Mammography*, Springer, 421-427 (2010).
- [4] McKinley, R. L., Tornai, M. P., Tuttle, L. A., Steed, D. and Kuzmiak, C. M., "Development and initial demonstration of a low-dose dedicated fully 3d breast CT system", *Breast Imaging*, Springer, 442-449 (2012).
- [5] Agostinelli, S. et al., "Geant4: a simulation toolkit.", *Nuclear Instruments and Methods in Physics Research A*, 506, 250-303 (2003).
- [6] Poludniowski, G., Landry, G., DeBlois, F., Evans, P.M. And Verhaegen, F., "SpekCalc: a program to calculate photon spectra from tungsten anode x-ray tubes", *Physics in Medicine and Biology*, 54 (19), 433-438 (2009).
- [7] Buzug, T. M., [Computed tomography: from photon statistics to modern cone-beam CT], Springer Science & Business Media, 423-425 (2008).
- [8] de las Heras, H., Tischenko, O., Panzer, W., Xu, Y. and Hoeschen, C., "Modeling and testing of a non-standard scanning device with dose reduction potential", *SPIE Proceedings*, 6510, Medical Imaging, 2007, 65103R (2007).
- [9] Tischenko, O., Xu, Y. and Hoeschen, C., "Imaging method and device with dual reading scanner", European Patent EP1780676, filed on 25/10/2005 published on 02/05/2007.